# University of Birmingham

# Monitoring Rheological Changes Using Acoustic Emissions for Complex Formulated Fluids Manufacturing

Hefft, Daniel Ingo; Blake, Natasha Rosanne; Farhoud, Aziza; Farrar, Ellie; O'Sullivan, Jonathan James; Alberini, Federico

*Document Version*
Publisher's PDF, also known as Version of record

[Link to publication on Research at Birmingham portal](Link to publication on Research at Birmingham portal)

Daniel Ingo Hefft[1,2,*]

Natasha Rosanne Blake[1,3]

Aziza Farhoud[1]

Ellie Farrar[1,3]

Jonathan James O'Sullivan[3]

Federico Alberini[1,4,*]

# Monitoring Rheological Changes Using Acoustic Emissions for Complex Formulated Fluids Manufacturing

The measurement capabilities of a newly developed in-situ rheometric device based on a single passive acoustic emission sensor and machine learning algorithms were investigated. Two surfactant structured fluids demonstrating complex non-Newtonian rheology (Power-law and Herschel-Bulkley models) were examined. Furthermore, a static evaluation on the laboratory scale in comparison to dynamic processing on the pilot scale was conducted. The results indicate that the machine learning algorithms of this technology can identify, in > 90 % of scenarios, the correct type of rheology or the manufacturing process step across both scales. This identification is based on solving a classification problem using quadratic support vector machine learning algorithms, which have proven to deliver the most robust predictions across a choice of 24 different algorithms tested. Additionally, a new format of in situ rheology display was introduced, referred to as RRF™ factor.

## 1   Introduction

Many fluids that are produced on the industrial scale are multi-component, formulated products, where the rheology of these systems develops over the duration of the manufacturing process. The rheology that is demonstrated in most cases is typically non-Newtonian in nature [1], and its determination in situ during industrial-scale mass production could provide insights that would enable energy and time savings [2, 3]. Typical fluid behavior assessment techniques in the industry are either the use of in-line viscometry, which can have slow response times, or off-line viscometry and/or rheometry approaches, which can be time consuming [4, 5]. Within the fast-moving consumer goods (FMCG) industry, the measurement of rheology is essential as a quality indicator for a product [6, 7], as the consumer often links rheology to quality [8, 9]. A few examples include the routine rheology assessment of honey, being a known driving factor of organoleptic perception, which allows predictions on the honey quality to be made [10]. Furthermore, rheology measurements are a reliable tool to uncover adulteration of honey blended with other amorphous sugars, because rheology is such an inherent fluid property and adulteration leads to shifts of the expectable rheological profiles compared to pure, unadulterated honey [11]. In the beverage industries, rheology is measured for the assessment of emulsion stability and cloudiness of juice-type products (oil-in-water emulsions, where the oil is a combination of essential and vegetable oils [12]), in addition to the assessment of the foam stability of light and dark beers by off-line large-amplitude oscillatory shear measurements [13]. Off-line rheometry has been proposed as a tool to characterize lamellar-structured (colloidal) liquids in regard to their rheology (flow curves and yield stress) [14]. Processing conditions such as temperature, mixing intensity, and time have been mapped dynamically using a rotational rheometer, showing an approach to using a rheometer as a means to replicate the processing conditions on the laboratory scale.

Creating a product's rheological profile to assess the quality at the end of the manufacturing process is not the sole application of rheological testing. Its use during batch manufacture can provide unique insights for process understanding and

[1]Dr. Daniel Ingo Hefft ⓘ https://orcid.org/0000-0002-0775-7538
(D.I.Hefft.1@bham.ac.uk, Daniel.Hefft@campdenbri.co.uk),
Natasha Rosanne Blake, Aziza Farhoud, Ellie Farrar,
Prof. Federico Alberini
University of Birmingham, School of Chemical Engineering,
Edgbaston, Birmingham B15 2TT, UK.

[2]Dr. Daniel Ingo Hefft
Campden BRI, Station Road, Chipping Campden GL55 6LD, UK.

[3]Ellie Farrar, Dr. Jonathan James O'Sullivan
Unilever Research and Development, Port Sunlight Laboratory,
Quarry Road East, Bebington, Wirral CH63 3JW, UK.

[4]Prof. Federico Alberini (federico.alberini@unibo.it)
University of Bologna, Department of Industrial Chemistry,
Via del Risorgimento, Bologna 40136, Italy.

optimization, which could reduce the number of failed batches and minimize waste [15]. There is a lack of readily available in-line rheometry technologies for application to fluids exhibiting non-Newtonian rheological behavior and across a broad range of flow rates and scales of operation. Material wastage due to out-of-product specification rheology in manufacturing industries is thought to be ~5 % [16]. Hence, there is increasing interest to develop in-line rheometric devices that can reduce these losses and lead to more uniform product quality. Established methods of in-line viscosity determination include commercially available rotational viscometers [17, 18] and the use of differential pressure to derive the viscosity from the Hagen-Poiseuille equation [19, 20]. Both of these approaches give single viscosity values and are unable to capture the complexity of fluids possessing non-Newtonian rheological behavior. In recent decades, novel technologies with the potential to provide greater rheological insights in-line for industrial applications include electrical resistivity tomography (ERT) [21, 22] and ultrasound imaging velocimetry (UIV) [23, 24].

ERT itself is not a novel technology and was originally designed for geophysics and hydrology applications in order to explore the Earth's crust by measuring electrical voltage and current strength at the Earth's surface [25–27]. Be that as it may, in recent years ERT has been adopted for the measurement of complex rheology [28, 29], including food products (i.e., yoghurts [30]) and surfactant structured isotropic liquids (i.e., shampoo [31]), and to monitor emulsification processes in situ [32]. The system's outputs are displayed by time-lapsed images, allowing the derivation of, e.g., agitation times until homogeneity or rheological fluid characteristics.

UIV (commonly used along with pressure drop measurements [33]) is another prominent in-line rheometry technique used to monitor the rheology of complex fluids [34, 35], and has been validated on personal care products, namely shampoo [36]. The outputs from such measurements are velocity profiles over length, allowing the derivation of rheology. Ultrasonic technologies are classified as non-destructive, and as they are an emitter-receiver system, they are also often coined as an active acoustic emission (AE) technology [37]. Ultrasonic waves are pulsed in short bursts into the fluid, where the fluid will propagate the ultrasonic wave. A key assumption for UIV is the presence of heterogenicity, hence limiting the types of fluids suitable for this technology. If there are solid particles or bubbles present in the sound field, the sound wave will be attenuated by these systems. Part of the sound energy is scattered back to the ultrasonic transducer; this is dependent on the size and emission characteristics of the particle/bubble. However, there are multiple weaknesses in the technology. Standard UIV is only capable of measuring the velocity parallel to the ultrasound beam. Under the assumption of parallel flow, this only works when the angle between the ultrasound beam and the flow direction are known; direct proportionality between velocity component and velocity magnitude applies. In practical terms, this makes it either necessary to pre-condition the flow before passing by the transducer, or devices cannot be installed at restrictions, openings, or curves. Theoretically, an angle correction can be done; however, this is prone to error [38, 39]. There are limits to the possible gas and/or solid level within a fluid before the wave is fully scattered or adsorbed,

resulting in a loss of signal. Furthermore, UIV is restricted to a narrow range of flow rates, where the minimum flow rate possible is related to the resolution of the pressure drop sensor used, and the maximum flow rate is confined to a laminar flow regime. However, these are often not viable flow conditions in real industrial full-scale processes [40].

This study adds a new technology to the field of in-line rheometry; it is based on passive AE sensing and has been successfully subjected to patenting [41]. To the authors' knowledge, such a technology has yet to be used for the assessment of rheology in-line for non-Newtonian fluids on the laboratory and pilot scales. There has, however, been work carried out looking at the use of a single passive AE sensor flanged onto the outer wall of a pipe. Such studies focusing on AE in response to viscosity changes have been carried out on multiphase fluid systems exclusively, such as particulate slurries [42] and fluidized beds (solid-gas) [43]. Another application field for the above-mentioned technology is the detection of obstructions in pipe flow [44, 45], which may also be relevant for future applications to fouling detection and/or cleaning validation.

The objective of this work is to monitor the rheological changes of two formulated fluids exhibiting Power-law and Herschel-Bulkley rheological properties. This novel passive AE-based system comprises three major components. (1) The mechanical component consists of a metal pipe length with an inserted rod, serving as an "antenna" to receive and convey AE as the fluid passes through the duct. (2) The electronic component includes a single AE monitoring unit attached to a computer, which applies supervised machine learning models to classify different rheological states and processing conditions. The AE sensor is flanged onto the outer pipe wall, perpendicular to the extending rod and resting on a plateau. (3) The output user interface presents the rheological profile as a graphical fingerprint, introduced as the proprietary RRF™ factor. Results were validated against traditional off-line rheometry, and fluids have been processed on a static laboratory-scale and on a dynamic pilot-scale setup. The obtained results indicate that the machine learning algorithms of the technology can identify, in > 90 % of cases, the correct state of rheology and the process step across both equipment scales. The quadratic support vector machine (QSVM) algorithm proved to correctly classify the incoming AE data to this high level.

## 2 Materials and Methods

### 2.1 Materials

For the experiments on the laboratory scale, fluids were manufactured and kindly provided by Unilever R&D, Port Sunlight, UK. Five surfactant structured fluids that demonstrate non-Newtonian rheology were examined in this study. Three of the fluids exhibit Power-law rheological behavior and the other two fluids follow the Herschel-Bulkley model. Fluids for trials conducted on the pilot scale were not pre-manufactured, but manufactured in situ to dynamically map the process. Again, five fluids were manufactured similarly to those tested during the experiments on the laboratory scale and following the same principal rheological models.

## 2.2 Experimental Setup

Fig. 1 provides a schematic of the experimental setups on (a) the laboratory and (b) the pilot scale. Both experimental rigs consist of a recirculation loop with a tank, a pump, a flow-meter, and a 120-mm stainless-steel length of pipe with an internal diameter of 25.4 mm (1"). Both experimental rigs are comparable but differ in tank volume, achievable flow rates, thermal insulation, and mixing systems.

### 2.2.1 Laboratory-Scale Rig

The experiments were conducted in a closed recirculating system (Fig. 1a) fed by a 20-L conical tank powered by an APV DW1 series positive displacement pump (SPX FLOW Inc., USA). The flow rate was monitored by an OPTIMASS 700C Coriolis flowmeter (Krohne Ltd., UK). To detect the AE signals, the sensor was strapped onto the outer wall of a 130-mm DN25 (SCH 10) stainless-steel pipe segment on top of a circular pinhead that is connected to the tip of the geometry (T-shaped pin) – the modified pipe segment (Rheality Ltd., UK). This enables the sensing element not to be in direct contact with fluid, thus yielding advantages in both maintenance and hygiene if translated into an industrial environment. For each fluid, three fixed flow rates of 800, 1000, and 1200 L h$^{-1}$ were investigated. Acoustic measurements (see Sect. 2.4) for each fluid at all three flow rates were taken once the fluid had reached steady state. Steady state was reached when there was no flow rate fluctuation measured for 30 s. The recordings were repeated in duplicate for each fluid at each investigated flow rate.
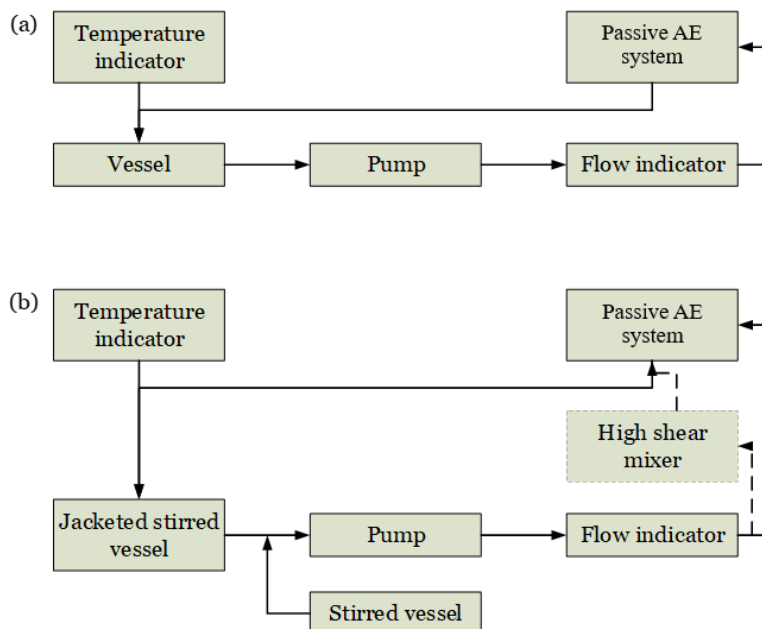
### 2.2.2 Pilot-Scale Rig

The pilot-scale rig was fed by a 50-L jacketed vessel fitted with an anchor scraper and a turbine impeller. This rig has the option to make use of an inline high-shear mixer within the recirculation loop. Acoustic measurements (see Sect. 2.4) were taken at each stage of production of the investigated fluids (Power-law and Herschel-Bulkley fluids), allowing the rheology of the process to be mapped by means of transient energy release measurements. Measurements were taken at the following stages at a fixed flow rate of 250 kg h$^{-1}$. Two different processes were used to manufacture the two products possessing disparate rheological properties. To produce the Power-law fluid, seven major process steps are involved, while for the Herschel-Bulkley-type fluid, five major steps are involved for their manufacture.

The following steps describe the manufacture of the formulated product possessing Power-law rheological behavior: (1) water addition, (2) main surfactant addition, (3) post surfactant minor I addition, (4) post surfactant minor II addition, (5) rheological modifier I addition – low-viscosity end product, (6) rheological modifier II addition – medium-viscosity end product, and (7) rheological modifier III addition – high-viscosity end product.

The following steps describe the manufacture of the formulated product possessing Herschel-Bulkley rheological behavior: (1) water addition, (2) addition of main ingredients, (3) addition of water, (4) addition of minor ingredients, and (5) high-shear mixing.

## 2.3 Rheology Characterization

The rheological material characterization was done with a Discovery HR-1 rheometer (TA® Instruments, Inc., USA), a rotational rheometer that can interchange geometries and Peltier element for temperature control. The fluids were tested in triplicate for the shear rates ranging from 0.1 to 1000 s$^{-1}$ and at a fixed temperature of 25 °C, using a vane-type geometry for the Power-law fluid (rotor vaned SST smart-swap with bob diameter 25 mm, bob length 42 mm, vane diameter 20.5 mm) and a 60-mm, 2° cone-on-plate geometry (stainless steel) for the Herschel-Bulkley-type fluids. The need to make use of the vane-type geometry is explained by the presence of slip and fluid viscosity. The results from this rheological characterization are presented in Tab. 1, showing that the two types of tested fluids follow either the Power-law or the Herschel-Bulkley relationship. Off-line rheological characterization was performed to identify the difference of the apparent rheological behavior. For simplicity, all fluids were fitted to the Herschel-Bulkley or Power-law model. Both are mathematically similar; however, the Herschel-Bulkley model considers an additional parameter: the yield stress. Power-law fluids follow the shear rate-stress behavior, given in Eq. (1).



**Figure 1.** Simplified experimental apparatus: (a) laboratory scale and (b) pilot scale. Dashed lines indicate the optional equipment/process stream that was used to determine the effects of the background noise.

$$\tau = K\dot{\gamma}^{n-1} \tag{1}$$

where $\tau$ is the shear stress (Pa), $k$ is the flow consistency index (Pa s$^n$), $\dot{\gamma}$ is the shear rate (s$^{-1}$), and $n$ is the flow behavior index (–). The Power-law formulation is not process dependent and, therefore, the final rheology should not be significantly affected by changes in the process temperature [46]. Herschel-Bulkley fluids follow the shear rate-stress behavior but incorporate a yield stress, as given in Eq. (2).

$$\tau = \tau_0 + k\dot{\gamma}^n \tag{2}$$

where $\tau_0$ is the yield stress (Pa), $k$ is the consistency index (Pa s$^n$), and $n$ is the flow index (–).

The measurements for the laboratory-scale experiments were carried out with fresh samples at the beginning of the first campaign of measurements, which were used as reference. For the pilot-scale trials, the measurements were carried out using samples collected during the trials. Tab. 1 details the rheological models and associated parameters for the investigated fluids.

## 2.4 AE Detection System

Transient energy releases were recorded using a PicoScope® 5243B oscilloscope (Pico Technology Ltd., UK). The transient recorder was attached to a Vallen AE sensing system (Vallen Systeme GmbH, Germany), comprising a DCPL2 decoupling unit, a 34-dB gain preamplifier, and a broadband sensor peaking at 375 kHz. The sensor itself is protected by an IP40-rated stainless-steel housing with a ceramic wear plate (sensitive area) of 20.3 mm in diameter. The sensor itself does not touch the fluid and rests on top of the pinhead of the modified pipe segment (Rheality Ltd., UK). The entire system and data processing structure is subject to an international patent application and includes further descriptors and figures [41].

Data acquisition was based on the following parameter set in the oscilloscope. Each sampling run comprises 100 recordings, the so-called buffer; 100 buffers (consecutive waveform recordings) are the maximum memory yield possible based on the hardware resolution, number of samples per buffer, and frequency. Within each buffer a waveform was recorded every 1.264 µs. Tab. 2 summarizes the hardware settings of data acquisition (time-domain data).

**Table 2.** Data acquisition parameter settings for the oscilloscope used in experimental testing (PicoScope® 5243B).

| Parameter | Setting | Unit |
|---|---|---|
| Sample interval | 1.264 | µs |
| Sample rate | 791.1 | kHz |
| Number of samples | 799 139 | – |
| Hardware resolution | 16 | bit |
| Number of recordings per product/process stage | 100 | – |

## 2.5 Post-Acquisition Data Processing and Interpretation

All the data processing was performed in Matlab® (R2019B Update 6, MathWorks Inc., USA). By means of a fast Fourier transform, the time domain signal (time-voltage fluctuation) is converted into its frequency domain (frequency-intensity plot), following the expression by Cooley and Tukey [47] and being a very common first step in data processing of AE [48, 49].

$$f_{\mathrm{m}} = \sum_{k=0}^{2n-1} x_k e^{\frac{2\pi i}{2n} \cdot mk} \quad m = 0, \ldots, 2n-1 \tag{3}$$

where $f_{\mathrm{m}}$ is the discrete signal (Hz), $n$ is the size of its domain (–), and $k$ represents an integer ranging from 0 to $2n-1$ (–), and $x_k$ is the indexed input (–).

A major feature of the Rheality™ system is also the use of the simplified acoustic signal generated by the Rheality Rheological Factor (RRF™) proprietary function [41], giving a unique acoustic fingerprint of the fluid rheology. The RRF™ reduces the amount of raw data points into a sizeable format for fast computation. Each raw signal buffer contains nearly 800 000 individual data points in its time domain. Even after converting the signals through fast Fourier transform, the datasets still contain around 750 000 data points, while the RRF™ condenses these points further to 10 individual factors that are sufficient to allow the machine learning models to solve classification problems regarding fluid and rheological state.

The RRF™ acoustic fingerprints from the laboratory-scale trials will

**Table 1.** Summary of the rheological assessment using an off-line rheometer for Power-law and Herschel-Bulkley fluids on both the laboratory and pilot scales.

| Scale | Formulation | $R^2$ [–] | $n$ [–] | $k$ [Pa s$^n$] | $\tau_0$ [Pa] | Rheological model |
|---|---|---|---|---|---|---|
| Lab scale | Test fluid 1$_{\text{Lab scale}}$ | 0.99 | 0.07 | 34.6 | 1.56 | Herschel-Bulkley |
| Lab scale | Test fluid 2$_{\text{Lab scale}}$ | 0.95 | 0.03 | 28.5 | 1.61 | Herschel-Bulkley |
| Pilot scale | Test fluid 1$_{\text{Pilot scale}}$ | 0.98 | 0.37 | 21.2 | 1.32 | Herschel-Bulkley |
| Pilot scale | Test fluid 2$_{\text{Pilot scale}}$ | 0.92 | 0.16 | 20.3 | 1.33 | Herschel-Bulkley |
| Lab scale | Low-viscosity fluid | 0.98 | 0.03 | 1.01 | – | Power-law |
| Lab scale | Medium-viscosity fluid | 0.99 | 0.82 | 1.73 | – | Power-law |
| Lab scale | High-viscosity fluid | 0.99 | 0.87 | 7.12 | – | Power-law |
| Pilot scale | Low-viscosity fluid | 0.97 | 0.01 | 0.89 | – | Power-law |
| Pilot scale | Medium-viscosity fluid | 0.99 | 0.43 | 0.92 | – | Power-law |
| Pilot scale | High-viscosity fluid | 0.99 | 4.08 | 0.65 | – | Power-law |

be used to train an ensemble of 24 machine learning models, while a pilot-scale trial will be used to mimic the process conditions of the laboratory-scale trials and to test how the trained model will cope with data acquired from a different set of experiments (both campaign datasets coming from laboratory-scale experiments). All algorithms are designed to solve classification problems and were tested to identify the best learning algorithm giving the highest prediction accuracy. A 10-fold cross-validation was applied to protect the datasets from overfitting, an approach common in applied machine learning computer sciences [50, 51]. All learning algorithms fall into one of the following classification learner categories: (1) decision trees (fine, medium, coarse), (2) discriminant analysis (linear, quadratic), (3) naïve Bayes (Gaussian, kernel), (4) support vector machines (SVM) (linear, quadratic, cubic, Gaussian (fine, medium, coarse)), (5) nearest-neighbor (nn) analysis (fine, medium, coarse, cosine, cubic, weighted), and (6) ensemble learners (trees (boosted, bagged, RUS boosted), subspace (discriminant, $k$-nn)). The quadratic SVM (QSVM) algorithm was found to deliver the highest prediction accuracies, meaning a correct classification between the real state of the fluid versus the predicted state based on the transformed AE signal input.

For the study of in-pipe obstruction presence predictions, QSVM has shown to be reliable [44]; hence, the algorithm itself has already proven a good degree of robustness when applied to fluid flow applications. Some of the advantages of QSVM include that it is a global optimization method; so, there are no local minima. It also avoids overfitting when moving into higher-dimensional spaces and makes good use of the kernel (separation of general learning principles and domain knowledge). As most problem-solving tasks are nonlinear, this algorithm is much more suited to handle complex datasets, unlike linear learning models. However, as the application of such a sensor to complex fluids had not been tested before, all 24 learning algorithms were tested. Using QSVM also minimizes error within measurements errors or the overlap of classes, given that QSVM include slack variables that have been designed to identify outlier values as such and do not use them as a basis for classification (unlike non-SVM models).

The training for the QSVM model of the laboratory-scale experiments took 3.2537 s with a one-versus-all method. This method transforms a multi-class problem into a binary problem, meaning that every possible pair of classes is respected. The one-versus-all method is less prone to the creation of imbalanced prediction models [52] and, hence, has been deemed as the superior method for the algorithm training. The prediction speed of the trained systems is 3300 observations per second and the confusion matrix, a tabular summary of predicted classes versus true classes, came back clean. This makes the created model comparably fast compared to less sophisticated algorithms such as SVM [53], meaning that the prediction speed is reasonable if this algorithm were deployed for an industrial application.

After the training stage, the created machine learning model was exported into the Matlab® workspace, where the model was tested on a second full set of processed AE in RRF™ format from a fully independent test campaign (second campaign), but on the same settings and the same fluids as per the first test campaign (training data). This will show how the model copes with previously unseen information and will validate the model's capabilities. For the validation of the single measurement campaign conducted on the pilot scale, a Pareto split of the dataset was applied: 80 % of data was used to train the algorithms, 20 % to validate the algorithm [54].

## 2.6 Data Collection and Curation

### 2.6.1 Rheological Characterization

Rheometer fluid characterization was performed in triplicate. The arithmetic mean was applied to determine the parameters of the Herschel-Bulkley and Power-law models.

### 2.6.2 Test Campaign

The data from the laboratory-scale testing was recorded in duplicate. The supplied formulations were divided into different aliquots to ensure that each day of experimentation used only virgin sample material. This step is necessary to ensure that the sensor system captured data on a consistent product and not on pre-sheared formulations from the previous trials. Pilot-scale testing was not repeated as the sensor system was primarily applied here for validation purposes to cope with scale-up. Furthermore, the batch quantities of the pilot scale made replicates very time intense as well as cost prohibitive.

### 2.6.3 Machine Learning

For the much larger datasets, created from the experiments on the laboratory-scale fluid circulation loop, the data was split into two groups (test campaigns 1 and 2). Campaign 1 represents a full dataset that was used to train machine learning models, while campaign 2 represents an independent dataset of new data to test the module; i.e., this is the part of the dataset that has not been involved in the weight creation and refinement of the machine learning algorithms. Weights are numerical factors that are used by machine learning algorithms to classify different rheology groups and fluid states. As for the pilot scale, the data was split according to the Pareto principle [54]. At random, 80 % of the data was used for the training phase of the algorithms while the remaining 20 % were used to test the created models on previously unseen data.

## 3 Results and Discussion

The results and discussion are split into two parts, where the first part presents the testing conducted on the laboratory-scale rig, examining if the passive AE sensor was capable of working well with multi-component formulated fluids demonstrating complex non-Newtonian rheological behavior (see Tab. 1). These laboratory-scale experiments described the initial testing of the pre-manufactured formulations, delivering a training dataset for the creation of machine learning models and the selection of the best-performing classification algorithm.

Furthermore, the laboratory setup was comparable to the one used on the pilot scale (see Fig. 1), but runs with different flow rates and temperatures were explored.

The second part details the findings on the validation of the passive AE technology applied on a pilot-scale setup. The aim of the validation experiments was to demonstrate the capability of the passive AE device and its potential to be deployed into an industrial setting. The processed AE were converted into the RRF™ format and were fed into the created machine learning model from the laboratory-scale experiments, to test the technology's capability and the algorithm's robustness. A key difference between the laboratory-scale and pilot-scale experiments is that the pilot-scale process was dynamic and the technology tracked the product manufacture.

### 3.1 Laboratory-Scale Trials

Initially, three different flow rates of 800, 1000, and 1200 L h$^{-1}$ were tested for each of the formulations, and the RRF™-processed signals for the Power-law and Herschel-Bulkley fluids are shown in Fig. 2. The proprietary RRF™ signature is divided into ten different parameters (P1–10) and the results are displayed on a normalized scale that ranges from 0 to 1. Along the abscissa, the running numbers of time steps are listed, representing the different sets of buffers (recordings). One hundred of these time steps on the abscissa represent the three flow rates under investigation, and the effects of the flow rate on the processed signal are presented in Fig. 2.

Low degrees of variation were observed for the testing conducted at flow rates of 800 and 1000 L h$^{-1}$, whereas greater fluctuation was exhibited for a flow rate of 1200 L h$^{-1}$, across both Power-law (17, number of recordings out of 300) and
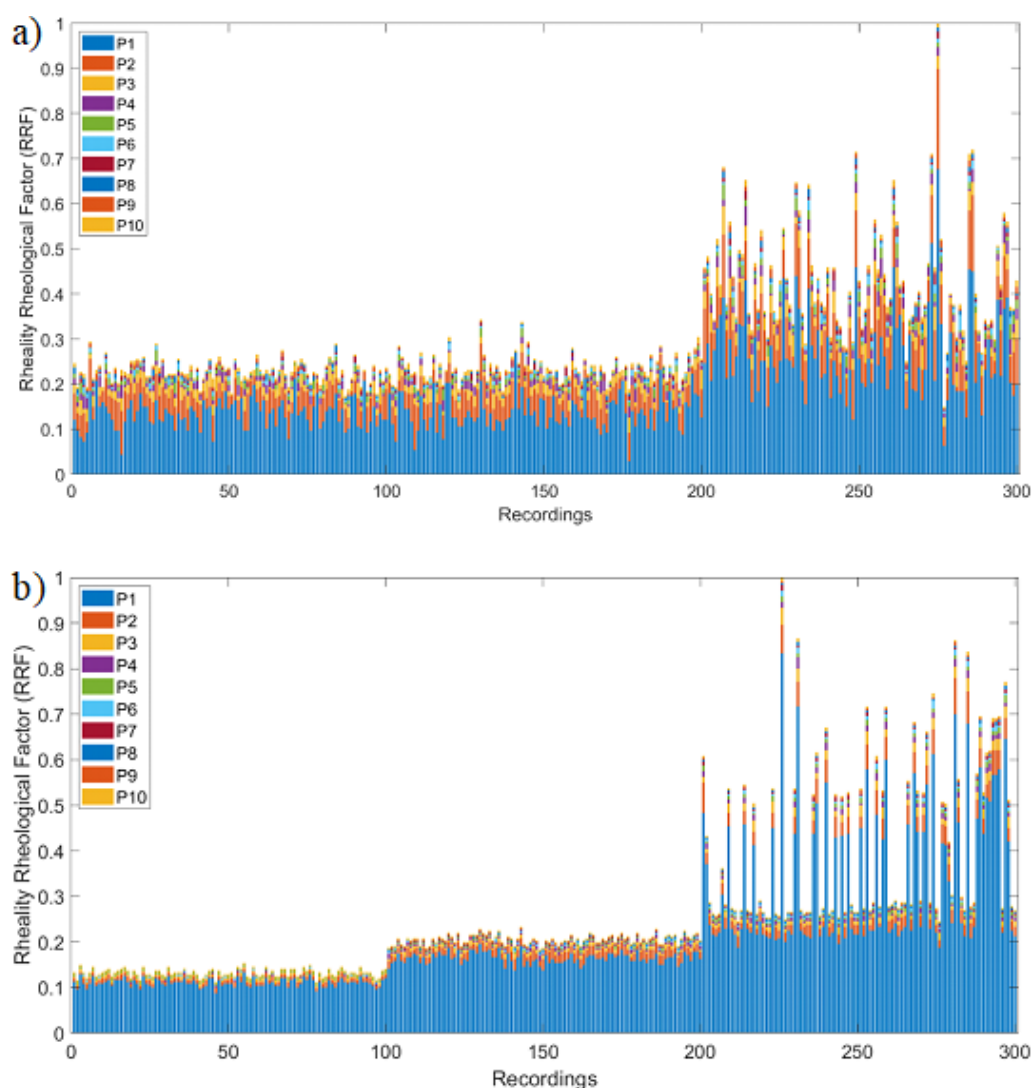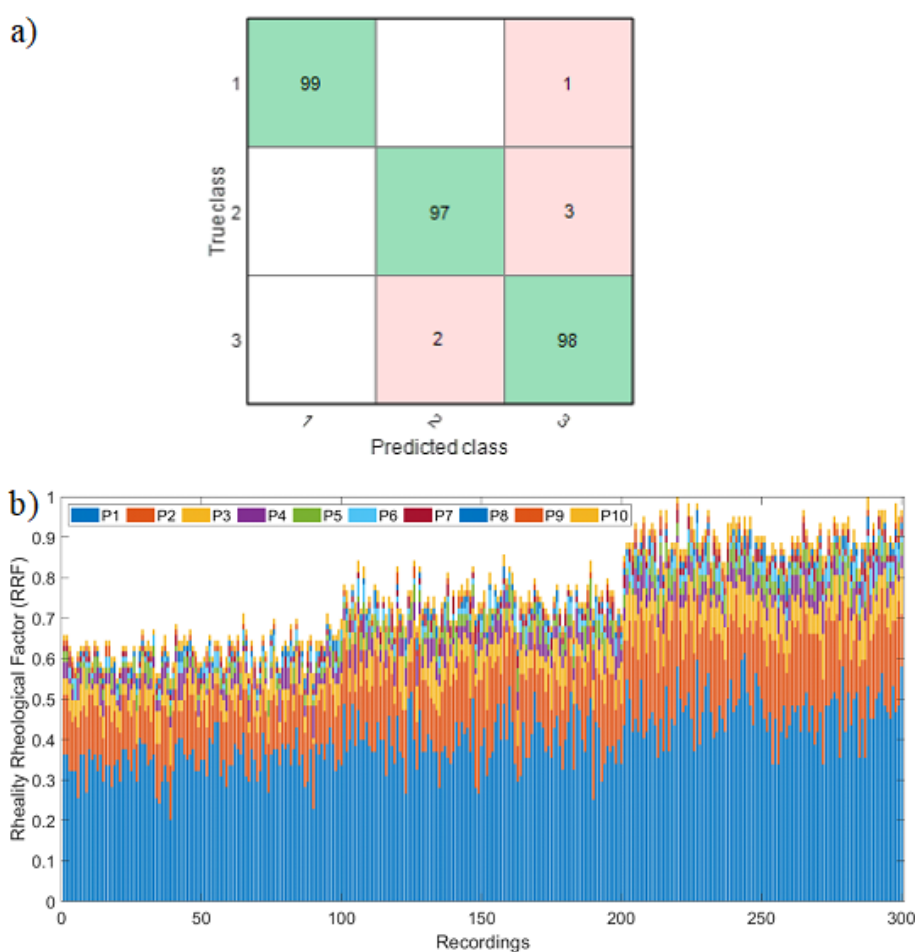


**Figure 2.** RRF™ results of each buffer across three different flow rates for (a) the Power-law and (b) the Herschel-Bulkley fluids. Recordings 1–100 represent 800 L h$^{-1}$, recordings 101–200 represent 1000 L h$^{-1}$, and recordings 201–300 represent 1200 L h$^{-1}$.

Herschel-Bulkley fluids (35, number of recordings out of 300). This behavior was thought to be associated with the occurrence of pump cavitation in the system at higher flow rates, which was exacerbated by the high viscosities of the investigated fluids, resulting in pumping inconsistencies causing pressure fluctuations and affecting the flow rate. Such AE bursts driven by cavitation in pipe flow have also been reported in the literature [55]. Moreover, greater overall variability was observed for the Power-law fluid (Fig. 2a) in comparison to the Herschel-Bulkley fluid (Fig. 2b), and this is thought to be associated with formulation differences between the two investigated fluids.

Since these inconsistencies of pumping or cavitation will cause fluctuations in pressure, the pressure-sensitive piezoelectric element will gather varying energy signatures (AE bursts). However, when considering a pilot plant processing environment, measurements would be taken consistently, and even if such fluctuations appeared, the effect on the overall reading would be minor, when averaged over the time of long production runs (signal smoothing [56]). Additionally, certain machine learning models can be used that can cope with unexpected data point outliers (slack) and would disregard these signals. It is therefore reasonable to deduce that considering these outliers would allow for the identification of pump overdrives at early stages and the identification of a most suitable pump type for certain types of fluids, or the optimal pump operation range for newly developed formulations.

When considering the case of the high-viscosity Power-law formulation (see Tab. 1), the flow appears stable across all transient recordings (Fig. 3). Fig. 3a shows the machine learning output expressed by a confusion matrix. A confusion matrix is a tabular expression of machine learning outputs that summarizes the number of predicted results (the algorithm's guess) versus the true class (the true condition). It also highlights the number of "confusions" where the algorithm has predicted a different class versus the true condition. Fig. 3b shows the corresponding expression in RRF™ format (the output of a proprietary simplification algorithm of processed AE as a 10-parameter expression, as in contrast to a complex Fourier transform of multiple 100 000 data points). QSVM (2.9122 s training time) gives robust prediction accuracy responses (Fig. 3a) in the region of 98 % (average of all 24 learning algorithms: 77.9 %), at a prediction speed of 2600 observations per second.



**Figure 3.** (a) Confusion matrix of the trained algorithm (class 1 = 800 L h$^{-1}$, class 2 = 1000 L h$^{-1}$, class 3 = 1200 L h$^{-1}$). (b) RRF™ results of each buffer across three different flow rates for the high-viscosity Power-law fluid. Recordings 1–100 represent 800 L h$^{-1}$, recordings 101–200 represent 1000 L h$^{-1}$, and recordings 201–300 represent 1200 L h$^{-1}$.

In addition, Figs. 2 and 3b show that increases in the flow rate lead to stronger transient energy releases and, hence, more intense RRF™ signatures. This effect of the flow rate on the AE signal intensity has been reported for Newtonian fluids [44, 45]; however, it can now be confirmed that the same trend appears for fluids demonstrating complex non-Newtonian rheology. These step changes appear smoother for the Power-law formulation when compared to the Herschel-Bulkley fluid, and this is thought to be associated with differences in the formulations between the two investigated fluids. Additionally, analyzing the parameter consistency in Fig. 2, the RRF™ parameter P1 does not change significantly across all investigated flow rates, suggesting that it is an underlying parameter, while parameters P2 and P3 vary the most with increasing flow rate. Since each of the color bands represents a certain processed part of the frequency spectrum, flow rate changes seem to be expressed by these parts of the frequency domain whereas the remaining parameters (P4–10) are associated with fluid rheology.

For the laboratory-scale experiments, two datasets were created. During the first test campaign, a full dataset was recorded

on which machine learning models were trained. Once trained, the model was tested against independent data from a second test campaign (test dataset). Fig. 4 shows the RRF™ signatures as well the confusion matrices at a fixed flow rate of 800 L h⁻¹. The results have 300 columns along the *x*-axis, where columns 1–100 represent the low-viscosity Power-law fluid, columns 101–200 the medium-viscosity Power-law fluid, and columns 201–300 the high-viscosity Power-law fluid (see Tab. 1).

Similar to Fig. 2, some outliers can be seen across both test campaigns (Fig. 4b and 4d). The chosen algorithm was QSVM (94.7 % prediction accuracy versus 67.8 % average of all other 24 investigated models). When testing the trained model on the data collected during the test dataset, the system was able to classify correctly 100 % of the data. Therefore, the data across the campaign was comparable, and both time and repeated shear do not seem to have an adverse impact on the rheology of the investigated Power-law fluid.

Fig. 5 shows the same plots as in Fig. 4 for the Herschel-Bulkley fluid, where distinct differences were observed in comparison to the Power-law fluid.

The initial algorithm is capable of distinguishing all the different cases of the Herschel-Bulkley fluid (see Tab. 1); however, when exposing the learning algorithms to the test dataset, which was collected after additional processing of the same sample, the ability of the model to achieve correct classifications drops to 74.7 % (the arithmetic mean value of correct classifications across all three classes as per Fig. 5b). This reduction in the model accuracy was thought to be associated with overprocessing of the Herschel-Bulkley fluid, where the microstructure of the product is altered as a consequence. Furthermore, more pump inconsistencies were observed and were comparatively negligible; yet, the rheological RRF™ differs immensely between both campaigns (Fig. 5b and 5d).

### 3.2 Pilot-Scale Trials

Prior to the formulation experiments on the pilot scale, the efficiency of filtering out environmental noise was investigated. This is a necessary step as there are known factors that can influence the frequency domain. These factors include valves [57], obstructions [45], leakages [58], and machinery wear and faults [59]. A trial with glycerol (30 °C) at a fixed flow rate of 250 L h⁻¹ was conducted. Initially, glycerol was pumped through the recirculation loop without the inline high-shear mixer in operation, and for a second test it was switched on to induce additional noise, both in terms of increased audible background noise and potential vibrations to the pilot-scale rig itself. No noticeable differ-
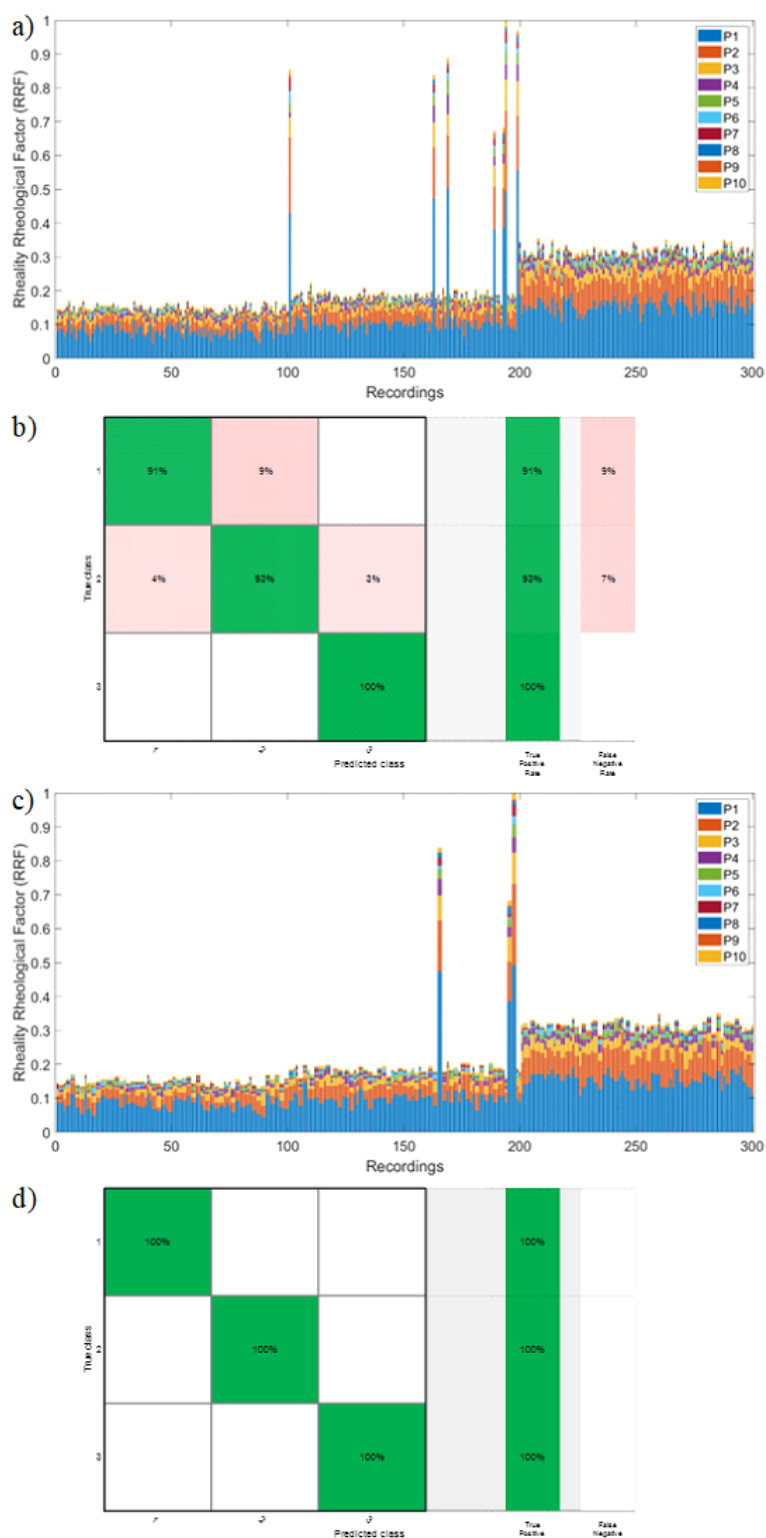


**Figure 4.** (a) RRF™ signatures for the training dataset, (b) its resulting training confusion matrix, (c) the RRF™ signatures of the test dataset, and (d) the confusion matrix results of the test dataset on the trained algorithm based on training data originating from the training dataset. Recordings 1–100 represent the low-viscosity Power-law fluid, recordings 101–200 represent the medium-viscosity Power-law fluid, and recordings 201–300 represent the high-viscosity Power-law fluid.
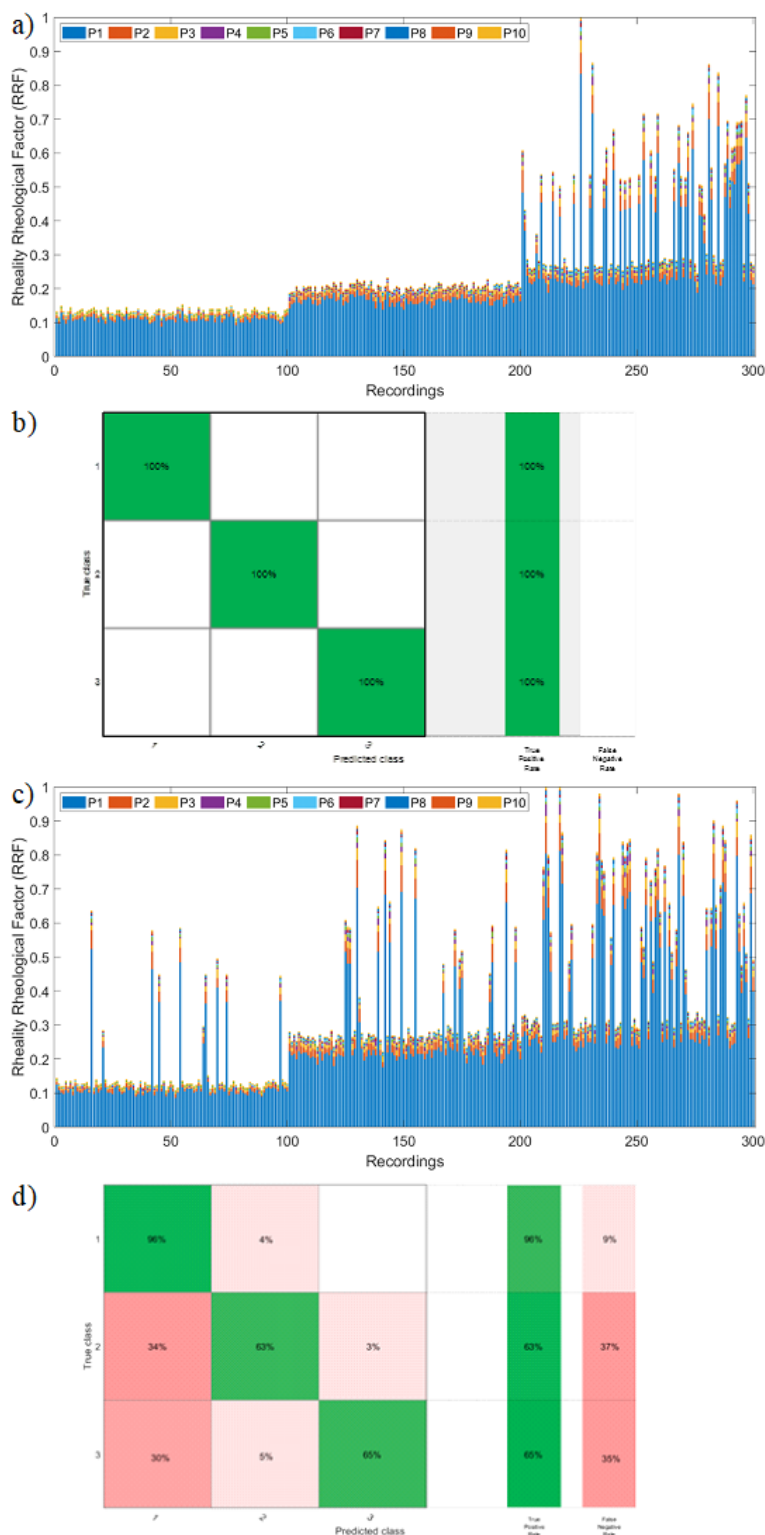
**Research Article**

**Figure 5.** (a) RRF™ signatures for the training dataset, (b) its resulting training confusion matrix, (c) the RRF™ signatures for the test dataset, and (d) the confusion matrix results of the test dataset on the trained algorithm based on training data originating from the training dataset. Time steps 1–100 represent 800 L h⁻¹, 101–200 represent 1000 L h⁻¹, and 201–300 represent 1200 L h⁻¹.

ences were observed between the two datasets, indicating that the signal selection and filtering effectively captures only the interaction between the passive AE sensor and the fluid, and no other events. This can be seen in Fig. 6 with transient recordings displayed in their frequency domain, after filtering.

Furthermore, Tab. 3 compares the key statistical indicators of the frequency for the scenarios where the in-line high-shear mixer is either off (Fig. 6a) or on (Fig. 6b). These results were created by using the Matlab® (R2019B Update 6, MathWorks Inc., USA) statistical analysis function and highlighted that, although background noise was audible to individuals conducting the experimental testing due to the in-line high-shear mixer being in operation, it did not influence the measurements for the passive AE measurement device. This behavior was attributed to the low frequency of the generated sound, outside the range of interest for the passive AE sensor measurements.

During pilot-scale testing, the passive AE sensor system achieved better classification when compared to the laboratory scale (see Figs. 4 and 5). The system was able to correctly distinguish 100 % of all manufacture stages (training and test stages), highlighting that the RRF™ is an effective tool for in-process implementation. The high accuracy of the achieved algorithms on the pilot scale is thought to be associated with the higher degree of process control across both temperature and flow rate measurements, in contrast to the laboratory environment. Furthermore, laboratory-scale testing utilized pre-manufactured fluids, where the rheology may have changed due to transport, storage, and re-shearing. This is also supported by comparing the differences in rheology (Tab. 2). However, the higher level of inaccuracy is not driven by the device's failure to measure, but the machine learning model attached to the passive AE sensor failing to deliver a better classification. A solution to this might be the use of improved models [60], more learning iterations [61], or to look at fuzzy networks [62].

For example, when considering the low-, medium-, and high-viscosity Power-law fluids, the RRF™ readings are very consistent and no significant outliers are observed (1 %) (Fig. 7).

For the Herschel-Bulkley product, two products were manufactured with the same formulation, where the two-endpoint rheology results were achieved through process alterations (a combination of varying both the temperature and the mixing conditions). Fig. 8 shows both processes with their mean RRF™ signatures for each process step.

The comparisons between the two batches show clear differences in the RRF™ signatures throughout the processes and a significantly different final product acoustic fingerprint (Fig. 8;
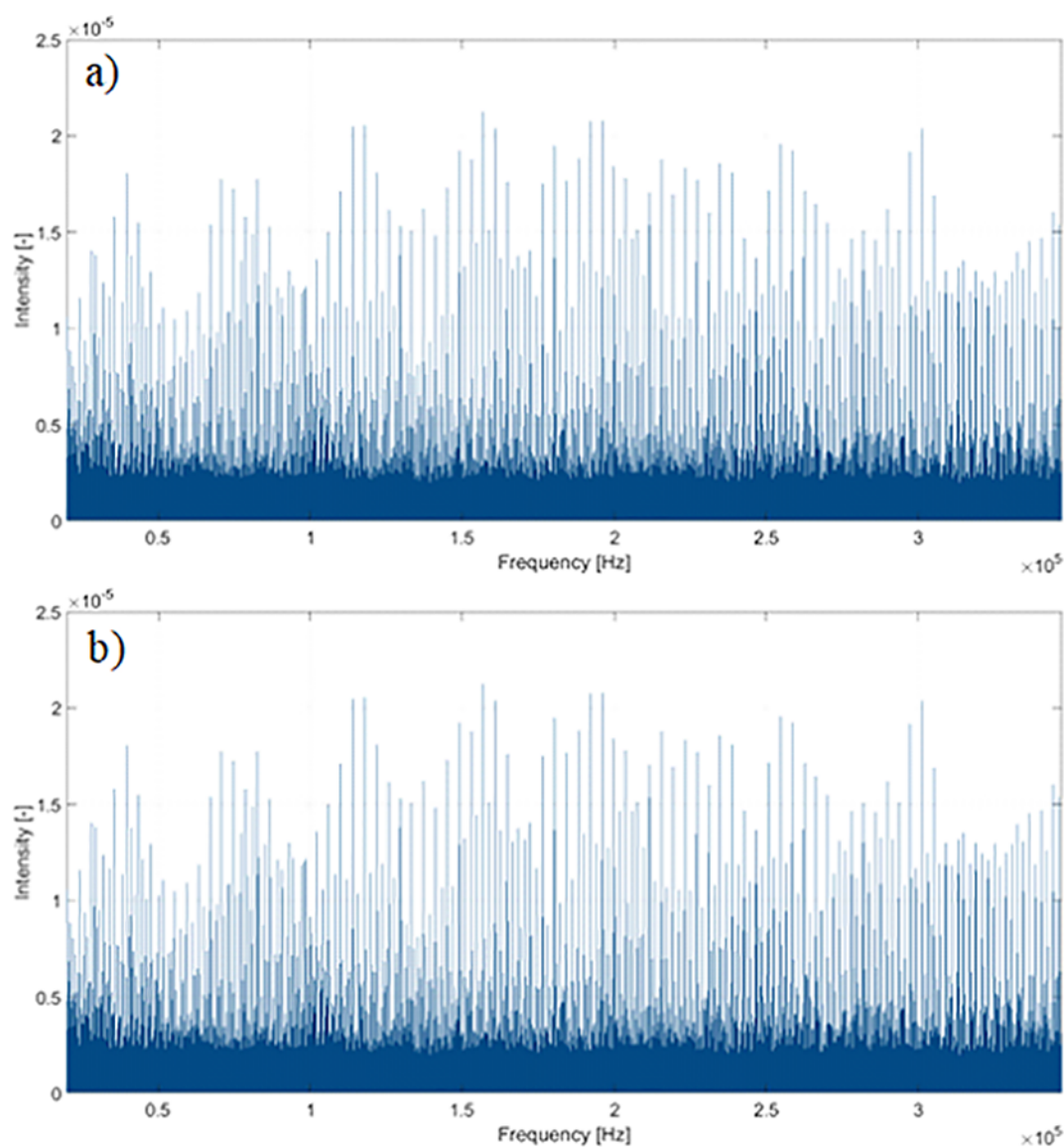
**Figure 6.** Frequency domains (fast Fourier transformed signals) of bandpass-filtered signals with (a) the in-line high-shear mixer switched off and (b) the in-line high-shear mixer switched on.

**Table 3.** Key statistical parameters of the frequency domain signals of Fig. 6.

|                    | (a)        | (b)        |
|--------------------|------------|------------|
| Minimum            | 0          | 0          |
| Maximum            | 2.1235e-05 | 2.1243e-05 |
| Mean (arithmetic)  | 9.7265e-07 | 9.7914e-07 |
| Median             | 8.5341e-07 | 8.6673e-07 |
| Standard deviation | 8.1515e-07 | 8.1505e-07 |

process stage 5). This is also supported by the two products having different rheological profiles as per results from the off-line rheological measurements (Tab. 1). Furthermore, Fig. 8 shows the potential to trace process stages that could be improved. For instance, looking at the different readings for stage 2 (Fig. 8a; stages 2–9), the RRF™ signatures have reached a steady state around position 7 (top $x$-axis), providing the possibility to optimize that specific stage of the manufacturing process.

QSVM appears to perform very well when tested on randomly selected data (20 %, Pareto split) of the total data pool but, as mentioned in an industrial environment, the prediction accuracies across all learning algorithms are enhanced (Fig. 9). Fig. 9 shows gross values of overall prediction accuracies based on the output of each machine learning model. The higher pre-
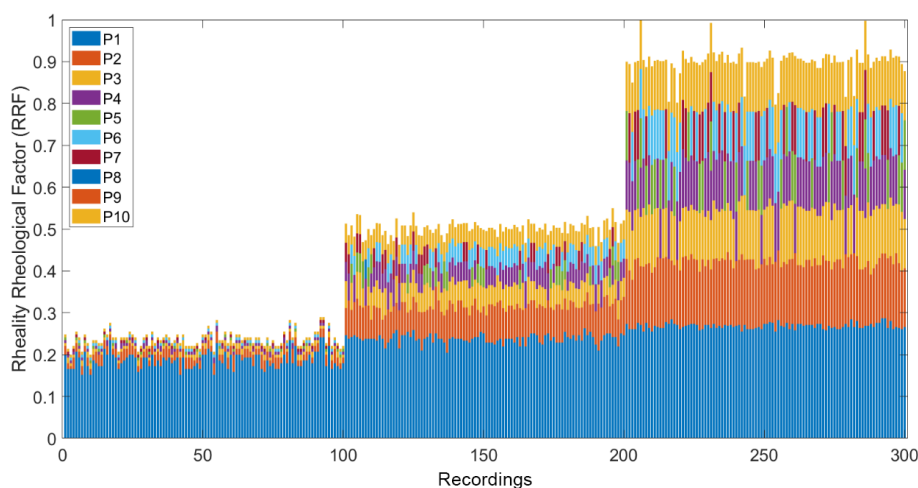
**Figure 7.** RRF™ signatures for pilot-scale data for the Power-law fluid. Recordings 1–100 represent the low-viscosity fluid, stages 101–200 represent the medium-viscosity fluid, and stages 201–300 represent the high-viscosity fluid (see Tab. 1).
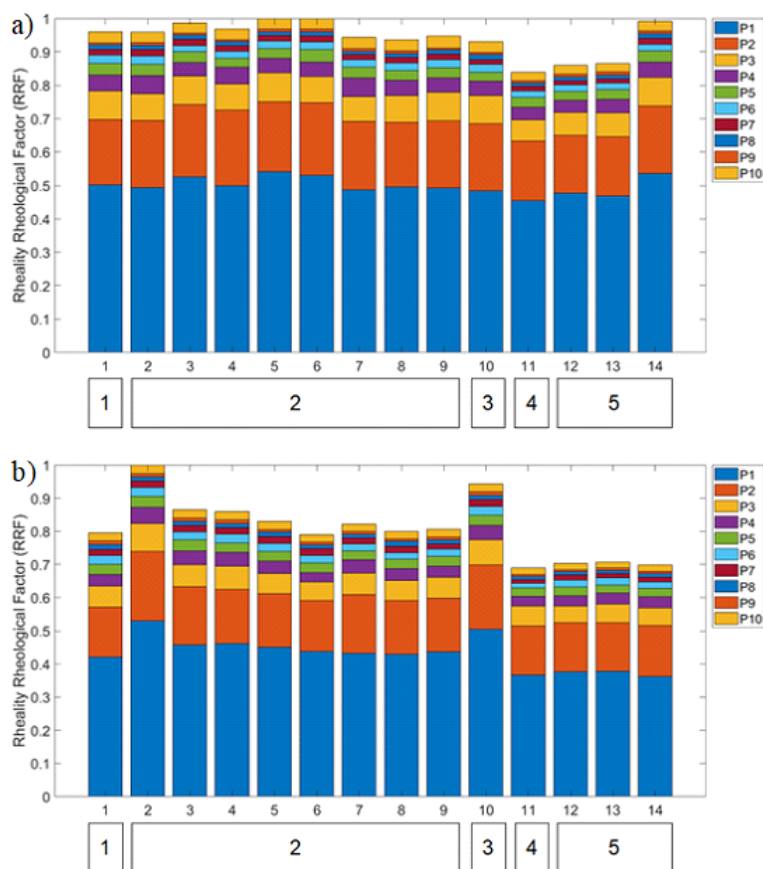
diction accuracy yields when conducting tests on the pilot scale are most likely due to the better process control and steadier process conditions when compared to the laboratory-scale setup.

Regularity in data is known to drive towards higher machine learning prediction accuracy [63, 64]. A preference for using QSVM remains in industrial applications, since this particular type of machine learning algorithm can cope better with outlier readings (slack) and makes use of a kernel function. It is less computationally costly, meaning that it requires less memory compared to decision trees, and it is one of the most popular learning algorithms in applications. This is also due to the fact that SVM are capable of solving both classification and regression problems [65].

## 4    Conclusions

Passive AE were detected by using a novel technology with the aims of monitoring the manufacture and rheological changes of complex fluids live and in situ by using a simplified output, which is then transferred to supervised machine learning algorithms. Surfactant structured fluids demonstrating Herschel-Bulkley and Power-law relationships were investigated for this study on the laboratory and pilot scales, using the passive AE, and offline rheometry was conducted to validate the obtained rheological properties. On the pilot scale, the system was additionally tested to highlight that it was not impacted by environmental noise. Overall, QSVM delivered the best results, matching correctly > 90 % of scenarios and making very fast learning cycles and tests possible, unlike using the full information content of the time domain signals composed of 799 139 individual points. Nonetheless, the passive AE measurement system performs well in both laboratory- and pilot-scale environments and leads a step towards the reduction of the necessity for offline rheological testing for quality control testing in production environments, permitting batch cycle time reduction. Furthermore, the insights provided by this technology could enable better process understanding in situ, supporting waste reduction and optimization of energy consumption.
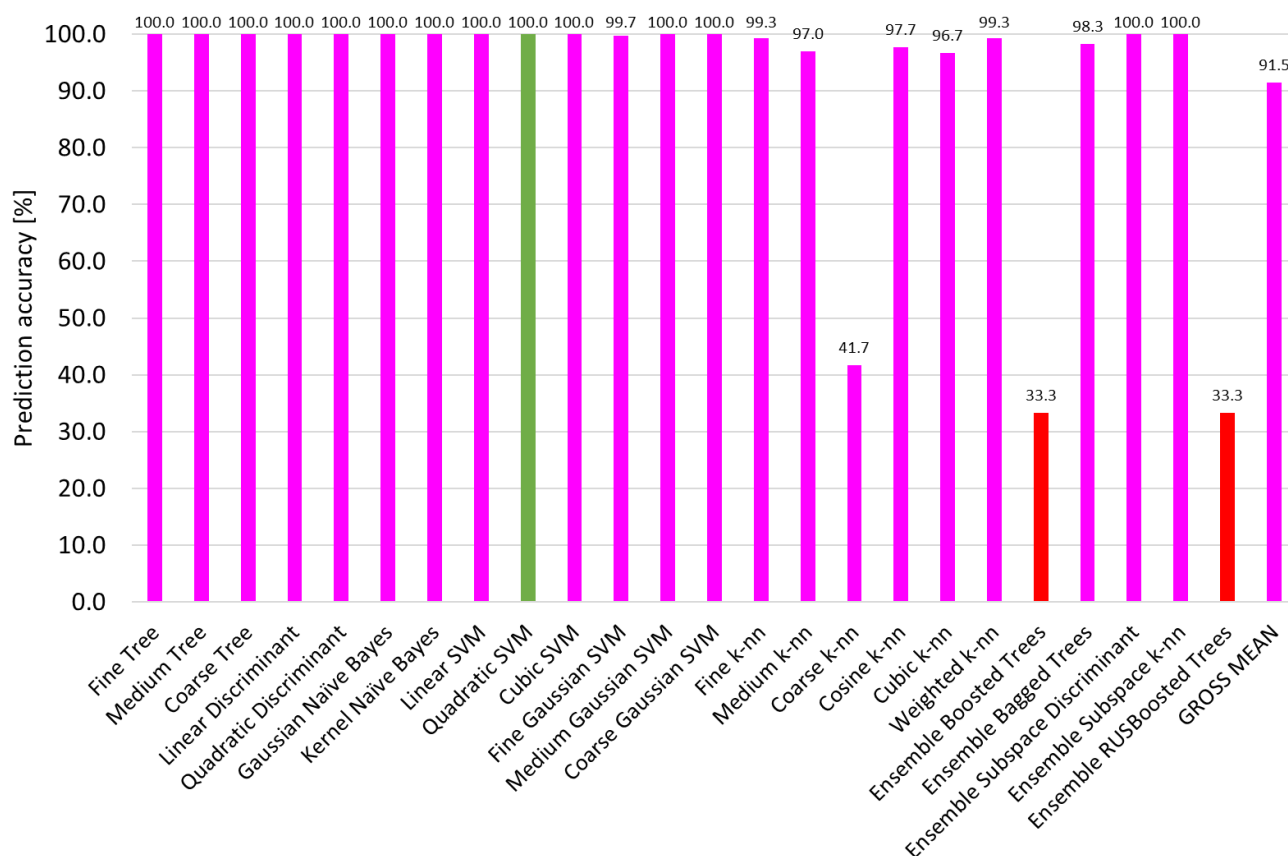


**Figure 8.** Averaged (top line of the x-axis) RRF signatures for the manufacture of (a) Test Fluid 1 and (b) Test Fluid 2 (Tab. 1). Bottom line of the x-axis mapped against process descriptors in Sect. 2.2.2.

**Figure 9.** Overview of the machine learning classification accuracy across all 24 algorithms for the manufacture of the investigated Herschel-Bulkley fluid.

## Conflict of Interests

The authors declare no competing interests. A patent has been filed by the University of Birmingham related to the acoustic acquisition technology for rheological measurements reported in this article, under PCT/GB2020/051548.

## Acknowledgments

## Abbreviations

| | |
|---|---|
| AE | acoustic emission |
| DN | Deutsche Normung |
| ERT | electrical resistivity tomography |
| $k$-nn | $k$-nearest neighbor |
| QSVM | quadratic support vector machine |
| R&D | research and development |
| RRF™ | Rheality Rheological Factor™ |
| SVM | support vector machine |
| UIV | ultrasound imaging velocimetry |

## References

[1] R. P. Chhabra, in *Advances in Heat Transfer* (Ed: J. P. Harnett), Vol. 37, Academic Press, Orlando **2003**.

[2] Y. J. Choi, K. L. Mccarthy, M. J. McCarthy, *J. Food Sci.* **2002**, *67 (7)*, 2718–2724. DOI: https://doi.org/10.1111/j.1365-2621.2002.tb08804.x

[3] *Applications in Electronics Pervading Industry, Environment and Society* (Eds: S. Saponara, A. De Gloria), vol. 573, Springer International Publishing, Cham **2019**.

[4] B. M. McKenna, J. G. Lyng, in *Woodhead Publishing Series in Food Science, Technology and Nutrition* (Ed: F. McKenna), Woodhead Publishing, Abington **2003**. https://www.sciencedirect.com/science/article/abs/pii/B9781855736733500114?via%3Dihub

[5] I. Roberts, in *Woodhead Publishing Series in Food Science, Technology and Nutrition* (Ed: F. McKenna), Woodhead Publishing, Abington **2003**. https://www.sciencedirect.com/science/article/abs/pii/B9781855736733500126?via%3Dihub

**Chemical Engineering & Technology**

**Research Article**

[6] H. A. Barnes, *Appl. Rheol.* **2001**, *11 (2)*, 89–101. DOI: https://doi.org/10.1515/arh-2001-0006

[7] A. Lindner, P. E. Arratia, *Biomicrofluidics* **2016**, *10 (4)*, 043301. DOI: https://doi.org/10.1063/1.4961681

[8] P. Fischer, E. J. Windhab, *Curr. Opin. Colloid Interface Sci.* **2011**, *16 (1)*, 36–40. DOI: https://doi.org/10.1016/j.cocis.2010.07.003

[9] J. Ahmed, P. Ptaszek, S. Basu, *Advances in Food Rheology and Its Applications*, Woodhead Publishing, Abington **2016**.

[10] G. Towler, R. Sinnott, in *Chemical Engineering Design: Principles, Practice and Economics of Plant and Process Design*, 2nd ed., Butterworth-Heinemann, Oxford **2013**.

[11] V. O. Anidiobu, *J. Apic. Res.* **2023**, *62 (3)*, 570–577. DOI: https://doi.org/10.1080/00218839.2021.1874708

[12] A. R. Taherian, P. Fustier, M. Britten, H. S. Ramaswamy, *Food Biophys.* **2008**, *3 (3)*, 279–286. DOI: https://doi.org/10.1007/s11483-008-9093-4

[13] M. Wilhelm, K. Reinheimer, J. Kübel, *Z. Phys. Chem.* **2012**, *226 (7/8)*, 547–567. DOI: https://doi.org/10.1524/zpch.2012.0247

[14] G. E. Cunningham, F. Alberini, M. J. H. Simmons, J. J. O'Sullivan, *Chem. Eng. Sci.* **2021**, *242*, 116752. DOI: https://doi.org/10.1016/j.ces.2021.116752

[15] C. Damian, *An. Univ. "Ovidius" Constanta, Ser.: Chim.* **2013**, *24 (1)*, 17–20. DOI: https://doi.org/10.2478/auoc-2013-0003

[16] J. M. Rees, *Adv. Colloid Interface Sci.* **2014**, *206*, 294–302. DOI: https://doi.org/10.1016/j.cis.2013.05.006

[17] N. Schneider, M. Gerber, *Renewable Sustainable Energy Rev.* **2020**, *121*, 109709. DOI: https://doi.org/10.1016/j.rser.2020.109709

[18] K. A. Abbas, A. Mohammed, A. M. Saleh, M. Ebrahimian, *J. Food Agric. Environ.* **2010**, *8*, 100–107.

[19] J. J. O'Sullivan, C. Schmidmeier, K. P. Drapala, J. A. O'Mahony, A. L. Kelly, *J. Food Eng.* **2017**, *197*, 9–16. DOI: https://doi.org/10.1016/j.jfoodeng.2016.10.023

[20] J. J. O'Sullivan, K. P. Drapala, A. L. Kelly, J. A. O'Mahony, *J. Food Eng.* **2018**, *222*, 218–225. DOI: https://doi.org/10.1016/j.jfoodeng.2017.10.015

[21] S. C. Low, D. Allitt, N. Eshtiaghi, R. Parthasarathy, *Chem. Eng. Res. Des.* **2018**, *130*, 42–51. DOI: https://doi.org/10.1016/j.cherd.2017.11.039

[22] G. Forte, A. Albano, M. J. H. Simmons, H. E. Stitt, E. Brunazzi, F. Alberini, *Chem. Eng. Technol.* **2019**, *42 (8)*, 1602–1610. DOI: https://doi.org/10.1002/ceat.201800728

[23] R. Kotzé, S. Ricci, B. Birkhofer, J. Wiklund, *Flow Meas. Instrum.* **2016**, *48*, 104–111. DOI: https://doi.org/10.1016/j.flowmeasinst.2015.08.013

[24] T. S. Awad, H. A. Moharram, O. E. Shaltout, D. Asker, M. M. Youssef, *Food Res. Int.* **2012**, *48 (2)*, 410–427. DOI: https://doi.org/10.1016/j.foodres.2012.05.004

[25] S. Hammer, *Geophysics* **1939**, *4 (3)*, 184–194. DOI: https://doi.org/10.1190/1.1440495

[26] R. Maillet, *Geophysics* **1947**, *12 (4)*, 529–556. DOI: https://doi.org/10.1190/1.1437342

[27] P. Sava, A. Revil, M. Karaoulis, *Geophys. J. Int.* **2014**, *198 (2)*, 880–894. DOI: https://doi.org/10.1093/gji/ggu166

[28] L. Pakzad, F. Ein-Mozaffari, S. R. Upreti, A. Lohi, *Can. J. Chem. Eng.* **2013**, *91 (1)*, 90–100. DOI: https://doi.org/10.1002/cjce.21616

[29] T. D. Machin, H.-Y. Wei, R. W. Greenwood, M. J. H. Simmons, *Chem. Eng. Sci.* **2018**, *187*, 327–341. DOI: https://doi.org/10.1016/j.ces.2018.05.017

[30] M. Henningsson, M. Regner, K. Östergren, C. Trägårdh, P. Dejmek, *J. Food Eng.* **2007**, *80 (1)*, 166–175. DOI: https://doi.org/10.1016/j.jfoodeng.2006.04.058

[31] Z. Ren, A. Kowalski, T. L. Rodgers, *Flow Meas. Instrum.* **2017**, *58*, 31–37. DOI: https://doi.org/10.1016/j.flowmeasinst.2017.09.013

[32] C. Tan, N. Wang, F. Dong, *J. Cent. South Univ.* **2016**, *23 (1)*, 240–248. DOI: https://doi.org/10.1007/s11771-016-3067-3

[33] Incipientus, Incipientus Ultrasound Flow Technologies AB, https://www.incipientus.com/, **2019** (accessed on October 14, 2019).

[34] D. Patel, F. Ein-Mozaffari, M. Mehrvar, *IOP Conf. Ser. Mater. Sci. Eng.* **2012**, *42*, 012048. DOI: https://doi.org/10.1088/1757-899X/42/1/012048

[35] S. Saeed, F. Ein-Mozaffari, S. R. Upreti, *Ind. Eng. Chem. Res.* **2007**, *46 (7)*, 2172–2179. DOI: https://doi.org/10.1021/ie0607548

[36] J. Wiklund, M. Johansson, J. Shaik, P. Fischer, E. Windhab, M. Stading, A.-M. Hermansson, in *Third Int. Symp. Ultrason. Doppler Methods Fluid Eng.*, Lausanne **2002**.

[37] J. W. R. Boyd, J. Varley, *Chem. Eng. Sci.* **2001**, *56 (5)*, 1749–1767. DOI: https://doi.org/10.1016/S0009-2509(00)00540-6

[38] K. Logason, T. Bärlin, M.-L. Jonsson, A. Boström, H. G. Hårdemark, S. Karacagil, *Eur. J. Vasc. Endovasc. Surg.* **2001**, *21 (4)*, 311–313. DOI: https://doi.org/10.1053/ejvs.2001.1331

[39] K. H. Fraser, C. Poelma, B. Zhou, E. Bazigou, M.-X. Tang, P. D. Weinberg, *J. R. Soc., Interface* **2017**, *14 (127)*, 20160761. DOI: https://doi.org/10.1098/rsif.2016.0761

[40] J. Wiklund, R. Haldenwang, R. R. Kotze, *Fluid Visualisation and Characterisation System and Method; a Transducer*, Google Patents **2016**.

[41] F. Alberini, D. I. Hefft, G. G. Forte, *Identifying Liquid Rheological Properties from Acoustic Signals*, WO2020260889A1, **2020**.

[42] R. Hou, A. Hunt, R. Williams, *Powder Technol.* **1999**, *106 (1/2)*, 30–36. DOI: https://doi.org/10.1016/S0032-5910(99)00051-0

[43] G. Book, K. Albion, L. Briens, C. Briens, F. Berruti, *Powder Technol.* **2011**, *205 (1–3)*, 126–136. DOI: https://doi.org/10.1016/j.powtec.2010.09.002

[44] D. I. Hefft, F. Alberini, *Biosyst. Eng.* **2020**, *191*, 48–59. DOI: https://doi.org/10.1016/j.biosystemseng.2019.12.015

[45] L. Baronti, M. Castellani, D. Hefft, F. Alberini, *Can. J. Chem. Eng.* **2022**, *100 (3)*, 521–539. DOI: https://doi.org/10.1002/cjce.24202

[46] B. Abu-Jdayil, H. A. Mohameed, M. Sa'id, T. Snobar, *Int. J. Cosmet. Sci.* **2004**, *26 (1)*, 19–29. DOI: https://doi.org/10.1111/j.0142-5463.2004.00201.x

[47] J. W. Cooley, J. W. Tukey, *Math. Comput.* **1965**, *19 (90)*, 297–297. DOI: https://doi.org/10.1090/S0025-5718-1965-0178586-1

[48] L. Zhao, L. Kang, S. Yao, *IEEE Access* **2019**, *7*, 984–993. DOI: https://doi.org/10.1109/ACCESS.2018.2886095

[49] W. N. Lopes, P. O. C. Junior, P. R. Aguiar, F. A. Alexandre, F. R. L. Dotto, P. S. da Silva, E. C. Bianchi, *Int. J. Adv. Manuf. Technol.* **2021**, *113 (1/2)*, 585–603. DOI: https://doi.org/10.1007/s00170-020-06476-3

[50] D. M. Hawkins, *J. Chem. Inf. Comput. Sci.* **2004**, *44 (1)*, 1–12. DOI: https://doi.org/10.1021/ci0342472

[51] M. N. Fienen, N. G. Plant, *Environ. Model. Softw.* **2015**, *63*, 14–23. DOI: https://doi.org/10.1016/j.envsoft.2014.09.007

[52] R. Akbani, S. Kwek, N. Japkowicz, in *Lecture Notes in Computer Science* (Eds: J. Boulicaut, F. Esposito, F. Giannotti, D. Pedreschi), Springer, Berlin, Heidelberg **2004**.

[53] A. Chakhar, D. Ortega-Terol, D. Hernández-López, R. Ballesteros, J. F. Ortega, M. A. Moreno, *Remote Sens.* **2020**, *12 (11)*, 1735. DOI: https://doi.org/10.3390/rs12111735

[54] A. Clark, *ISACA J.* **2018**, *1*, 1–6.

[55] S. Husin, A. Addali, D. Mba, *Flow Meas. Instrum.* **2013**, *33*, 251–256. DOI: https://doi.org/10.1016/j.flowmeasinst.2013.07.011

[56] S. Rippengill, K. Worden, K. M. Holford, R. Pullin, *Strain* **2003**, *39 (1)*, 31–41. DOI: https://doi.org/10.1046/j.1475-1305.2003.00041.x

[57] X. Qian, in *Int. Compress. Eng. Conf.*, Purdue University, West Lafayette **1986**.

[58] P. J. Lee, J. P. Vítkovský, M. F. Lambert, A. R. Simpson, J. A. Liggett, *J. Hydraul. Eng.* **2005**, *131 (7)*, 596–604. DOI: https://doi.org/10.1061/(ASCE)0733-9429(2005)131:7(596)

[59] F. Elamin, Y. Fan, F. Gu, A. Ball, *Adv. Mech. Eng.* **2010**, *2*, 495741. DOI: https://doi.org/10.1155/2010/495741

[60] T. Imam, K. M. Ting, J. Kamruzzaman, z-SVM: An SVM for Improved Classification of Imbalanced Data, in *AI 2006: Advances in Artificial Intelligence* (Eds: A. Sattar, B. Kang), Springer, Berlin, Heidelberg **2006**, pp. 264–273.

[61] P. K. Mallapragada, R. Jin, A. K. Jain, Y. Liu, *IEEE Trans. Pattern Anal. Mach. Intell.* **2009**, *31 (11)*, 2000–2014. DOI: https://doi.org/10.1109/TPAMI.2008.235

[62] G. A. Banini, R. A. Bearman, *Int. J. Miner. Process.* **1998**, *52 (4)*, 233–244. DOI: https://doi.org/10.1016/S0301-7516(97)00071-9

[63] G. Fenza, M. Gallo, V. Loia, F. Orciuoli, E. Herrera-Viedma, *Appl. Soft Comput.* **2021**, *106*, 107366. DOI: https://doi.org/10.1016/j.asoc.2021.107366

[64] H. van Halteren, J. Zavrel, W. Daelemans, *Comput. Linguist.* **2001**, *27 (2)*, 199–229. DOI: https://doi.org/10.1162/089120101750300508

[65] T. Oommen, D. Misra, N. K. C. Twarakavi, A. Prakash, B. Sahoo, S. Bandopadhyay, *Math. Geosci.* **2008**, *40 (4)*, 409–424. DOI: https://doi.org/10.1007/s11004-008-9156-6

**Research Article**

**Research Article:** Passive acoustic emissions were detected by a new rheometric device to monitor the manufacture and rheological changes of complex fluids, live and in situ; a simplified output was then transferred to machine learning algorithms. Power-law and Herschel-Bulkley model fluids were studied on the laboratory and pilot scales. Offline rheometry was used to validate the obtained rheological properties.

**Monitoring Rheological Changes Using Acoustic Emissions for Complex Formulated Fluids Manufacturing**

Daniel Ingo Hefft*,
Natasha Rosanne Blake, Aziza Farhoud,
Ellie Farrar, Jonathan James O'Sullivan,
Federico Alberini*